Analytical Study of Icing Simulation for Turbine Engines in Altitude Test Cells

C.E. Willbanks* and R.J. Schulz†
ARO, Inc., Arnold Air Force Station, Tenn.

An analysis was made of icing simulation for aircraft turbine engines in a direct-connect, ground test facility. The relative importance of simulating droplet-size distribution, liquid water content, and humidity for testing anti-icing systems was investigated. Calculations of the two-phase flow in a direct-connect facility was made in order to assess the relative importance of the duct inlet conditions on the establishment of a representative thermodynamic state of the flow at the engine inlet station for icing simulation. In addition, an analysis was made of the effects of the droplet distribution, liquid water content, and gas humidity on anti-icing power requirements in the test cell environment. The results of the study support the argument that the ground test facility provides a sufficiently realistic environment for turbine engine component anti-icing testing, and that the rest results will be representative of engine operation in atmospheric flight conditions.

Nomenclature

A = cross-sectional area of wind tunnel
b = sensible heat parameter, $W_c C_c / \bar{h}$
C = specific heat
C_D = droplet drag coefficient
C_p = constant pressure specific heat
C_v = mass fraction of water vapor
d = droplet diam
$\bar{d}$ = mass mean droplet diam
d_m = mass median droplet diam
E_c = internal energy of droplet
f_c = condensed phase loading factor, ratio of liquid water content to dry gas density
h = enthalpy
h_{fg} = enthalpy of phase change, liquid to vapor
$\bar{h}$ = heat transfer coefficient
k_x = mass transfer coefficient
L = liquid water content
M = Mach number
M_d = droplet mass
$\bar{M}$ = molecular weight
N = number density, droplets/unit vol
Pr = Prandtl number
p = static pressure
p_t = total pressure
p_v = vapor pressure
Q = heating rate parameter, $\dot{q}_s''/\bar{h}\ (T_s - T_r)$
$\dot{q}_s''$ = anti-icing heating rate
Re = Reynolds number
Ru = universal gas constant
Sc = Schmidt number
T = static temp, °R
T_f = droplet freezing temp
T_r = recovery temp of surface
T_s = surface temp
T_t = total temp
t = static temp, °K
V = velocity
W = mass flow rate
w_v = rate of evaporation
w_c = rate of subcooled liquid captured by surface
x = axial position
x_v = mole fraction of water vapor
γ = ratio of specific heats
μ = viscosity
ρ = density
ω = specific humidity

Subscripts

a = air
c = condensed phase, usually liquid
cs = condensed phase, solid, ice
e = boundary-layer edge conditions
g = gas mixture
i = droplets of class i, diam $= d_i$
nc = noncondensable gas, air
s = surface, usually liquid film surface
v = vapor phase
w = liquid water phase
w_t = total water mass
∞ = freestream conditions

Presented as Paper 73-1280 at the AIAA/SAE 9th Propulsion Conference, Las Vegas, Nevada, November 5-7, 1973; submitted November 18, 1973; revision received April 7, 1975. The research reported herein was conducted by the Arnold Engineering Development Center (AEDC), Air Force Systems Command (AFSC), Arnold Air Force Station, Tennessee, Research results were obtained by personnel of ARO, Inc., Contract Operator at AEDC. Further reproduction is authorized to satisfy the needs of the U.S. Government. The authors wish to acknowledge the help of Programer G.W. Lewis of CDPD at AEDC.

Index category: Airbreathing Engine Testing.

*Research Engineer. Now with Deering-Millikan Research Corporation, Spartanburg, S. Carolina.

†Research Engineer, Advanced Technology Section, Engine Test Facility.

Introduction

ICE accretion on aircraft components usually causes a degradation in the aircraft performance and operational safety. For this reason, aircraft are routinely equipped with either a system for intermittently removing the accumulated ice (a de-icing system) or a system for continuously maintaining the exposed surfaces free from ice (an anti-icing system). These systems must be tested under conditions which closely simulate, or if possible, duplicate naturally occurring icing conditions. There are three techniques currently used to conduct icing tests: flight testing under naturally occurring icing conditions; an artificial icing cloud created in the atmosphere by a tanker aircraft, or testing based on creating an

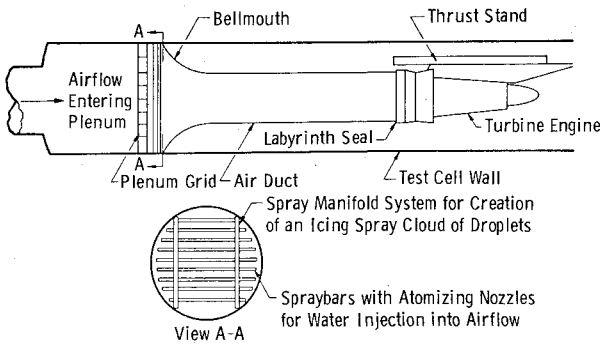

Fig. 1 Typical direct-connect propulsion engine altitude test cell configuration.

icing environment in a ground test facility or wind tunnel. The third technique as applied to the testing of aircraft turbofan engines is the subject of this paper.

In a recent state-of-the-art survey of icing simulation for aircraft turbine engines, Kissling[1] concluded that the ground test facility offers the best solution for icing simulation because all variables which define an icing condition can be controlled. A typical turbine engine test cell setup for icing simulation is shown schematically in Fig. 1. Water is injected into the cold airstream through air atomizing nozzles and the water droplets are accelerated to the airspeed by aerodynamic drag. Through heat and mass transfer, the droplets are cooled and approach near temperature equilibrium with the air. If the air temperature is sufficiently low, an environment simulating icing conditions which the engine experiences in the atmosphere can be created in the test facility at the turbofan inlet station.

In the present study, several aspects of the icing simulation problem are considered. Data on naturally occurring icing conditions and icing qualification specifications are briefly discussed. The degree of importance of correct simulation of some of the variables which characterize the icing environment is assessed and discussed. A one-dimensional analysis of the two-phase flow in a direct-connect type of facility is presented along with results obtained by this analytical method for typical icing test conditions.

Factors Affecting Icing Simulation

The specifications for icing testing, Table 1, can be made sufficiently definitive by specifying freestream static or total temperature and pressure, flight speed, freestream humidity, liquid water content, and a precisely defined mean effective droplet diameter. Ideally, a test cell for conducting engine icing tests should duplicate the flow conditions at the engine compressor face experienced by an engine in flight through an icing cloud. These flow conditions are therefore the proper air temperature, humdity, pressure, velocity, liquid water content, and droplet-size distribution. It is generally not practical and frequently impossible to duplicate all of the flow conditions encountered in atmospheric icing. Fortunately, however, it is not necessary to duplicate all of the icing conditions to get adequate simulation. A discussion of some of the factors affecting icing simulation follows.

Table 1 Icing conditions specified in the military specifications for turbojet and turbofan testing

Attribute	Condition I	Condition II
I. Sea-level anti-icing conditions		
Liquid water content	1 gm/m^3	2 gm/m^3
Atmospheric air temperature	−4°F(−20°C)	+23°F(−5.0°C)
Flight velocity	Static	Static
Altitude	Sea level	Sea level
Mean effective drop diameter	15 μ	25 μ
II. Altitude anti-icing conditions		
Liquid water content	0.5 gm/m^3	0.5 gm/m^3
Inlet air temperature	−4°F(−20°C)	−4°F(−20°C)
Flight velocity (Mach number)	0.32	0.71
Altitude	20,000 ft	20,000 ft
Mean effective drop diameter	15 μ	15 μ

Relation between Freestream and Engine Compressor Inlet Conditions

Since the flow conditions at the compressor face are rarely the same as the flight conditions, the air having been accelerated or diffused before entering the engine, it is necessary to relate the engine inlet conditions to the freestream conditions.

Analysis shows that flow from the freestream to the compressor inlet occurs at essentially constant specific humidity. Hence, the specific humidity at the compressor inlet in the test cell should be set equal to the specific humidity of the air at the flight conditions being simulated. In a natural icing cloud, it is assumed that the cloud is sufficiently homogeneous, at least on some local scale, that the supercooled liquid in the cloud is in equilibrium with its saturated vapor at the local ambient temperature. That is, the relative humidity in the cloud is 100%. Thus, the specific humidity at an engine compressor face is given by

$$\omega = \frac{\bar{M}_v}{\bar{M}_a} \frac{P_{v\infty}}{(P_\infty - P_{v\infty})} \tag{1}$$

where $p_{v\infty}$ is the saturation pressure of supercooled liquid at the freestream static temperature (T_∞) and p_∞ is the freestream static pressure, i.e., altitude pressure. The relative humidity at the compressor will be 100% only if the compressor inlet flow velocity equals the flight speed. Thus, the flow entering the compressor will generally not be in thermodynamic equilibrium.

Acceleration or deceleration of the flow from the freestream to the compressor inlet results in a change in the liquid water content. Two separate phenomena are involved, the compressibility of the gas, and droplet inertia, the inability of the droplets to follow streamlines exactly. The ratio of the liquid water content at the engine to the liquid water content in the freestream is known as the "scoop factor" which is a maximum under conditions of idle descent. The maximum value observed experimentally is approximately 1.3,[2] but higher theoretical values are possible.[3] Hence, the liquid water content probably changes by less than 30% from the freestream to engine face. In a following section it is shown that the power required to maintain an anti-icing condition is not highly dependent on liquid water content. Thus, the liquid water content of the flow in the test facility can be set equal to the freestream water content in most test cases, to obtain representative anti-icing power test results.

Effect of Droplet-Size Distribution on Surface Capture Efficiency

The droplets in a cloud do not follow straight line paths to the surface of an aerodynamic body in flight, rather, their trajectories are affected by the airflow around the body. The deviation of the trajectory of a droplet from a straight path depends on the droplet inertia and the flow conditions. Droplet capture efficiency of a surface is defined as the ratio of the actual rate of liquid impinging on a surface to the theoretical rate, obtained by assuming that the droplets follow straight paths. Since droplet trajectory is dependent on droplet inertia, hence drop size, the capture efficiency of a body is a function of droplet-size distribution as well as body shape and flow conditions.

The droplet-size distribution produced by air atomizing nozzles used in icing test cells is qualitatively similar to the distributions observed in natural clouds. Figure 2 shows a comparison of naturally occuring drop distributions $(N-a,N-b)$ with droplet-size distributions observed at the engine face in an icing test cell,[5] $(A-a,A-b)$. It can be noted that, for both the natural and artificially produced distributions, the peak mass fraction occurs near the mass median diameter. Obtaining a desired icing spray cloud with a distribution of air-atomizing spray nozzles located at the bellmouth or inlet of a direct test facility will, in most cases, require some experimentation. In most tests the object is to provide a uniform distribution of droplets, hence liquid water, in the flow at the engine inlet station.[5]

It is of interest to compare calculated capture efficiencies of typical turbofan engine components for these distributions. The capture efficiencies of small components, such as inlet guide vanes and blades, were estimated from capture efficiencies for circular cylinders obtained by Langmuir and Blodgett[6] taking the cylinder diameter to be equal to blade thickness. The spinner hub capture efficiency was estimated from existing solutions for flow over an ellipsoid of revolution.[7] Typical compressor inlet conditions were assumed; the results of the calculation are given in Table 2. Capture efficiencies for the cylinder are seen to be especially insensitive to droplet-size distribution. Moreover, the capture efficiency is even relatively insensitive to mass median droplet diameter. The capture efficiency of the ellipsoid is obviously highly dependent on the mass median droplet diameter. However, further analysis of the data indicates that the capture efficiency is not highly dependent on the size distribution for the same mass median diameter. The conclusion is that an adequate simulation of the mass mean or mass median diameter is the important simulation in performing icing tests in ground test facilities, with the simulation of the drop-size distribution being of relative, but not crucial importance.[3]

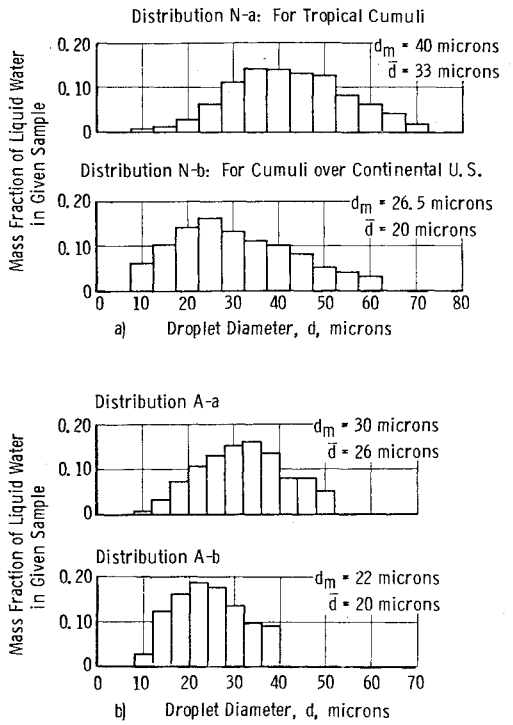

Fig. 2 Mass fraction of water contained in drops of given size class; a) natural environment; b) artificial environment.

Table 2 Calculations based on engine inlet conditions: velocity = 440 fps; pressure = 1932 psfa; temperature = 480°R.

Distribution (Fig. 2)	d_m, μ	Capture efficiency: Based on distribution	Capture efficiency: Based on mass median diameter
Cylinder diameter: 0.04166 ft (½ in.)			
A-b	22.0	0.909	0.912
N-b	26.5	9.923	0.925
A-a	30.0	0.938	0.942
N-a	40.0	0.928	0.962
Cylinder diameter: 0.25 ft (3 in.)			
A-b	22.0	0.632	0.630
N-b	26.5	0.690	0.680
A-a	30.0	0.725	0.732
N-a	40.0	0.770	0.805
5:1 Ellipsoid (10-ft major axis)			
A-b	22.0	0.072	0.055
N-b	26.5	0.107	0.079
A-a	30.0	0.119	0.110
N-a	40.0	0.180	0.160

Effect of Humidity, Liquid Water Content, and Liquid-Capture Rate on Required Anti-Icing Heating Rate

An analysis of the heating rate required to maintain an anti-icing condition on a surface in an icing environment was made.[3] The analysis is similar to the analysis of Neel, Bergum, Jukoff, and Schlaff[8] for the heat required to prevent ice formation on wings. From the analysis, information on the degree of importance of duplicating humidity, liquid water content, and liquid capture rate is obtained.

An anti-icing condition can be maintained if the surface is kept at a temperature slightly above the normal water bulk freezing point. The anti-icing heating rate can be determined from a heat balance at the surface considering heat loss by convection, sensible heating of the supercooled water impinging on the surface, and heat loss by vaporization of the water film that forms on the surface. Such an analysis yields the following equation, in nondimensional form, for the heat transferred across the anti-icing surface; specifically

$$Q=\frac{\dot{q}_s''}{\bar{h}(T_s-T_r)}=1.0+\frac{\dfrac{h_{fg}\bar{M}_v}{c_p\bar{M}_a}\left[\dfrac{P_r}{S_c}\right]^{0.67}\dfrac{(P_{v_s}-P_{v_e})}{P_e}+b(T_s-T_{c_\infty})-bT_e\dfrac{\gamma-1}{2}\dfrac{C_p}{C_c}M_e^2}{(T_s-T_r)} \quad (2)$$

The results of the analysis, for fixed T_{t_∞}, are shown in Figs. 3 and 4 for the flight conditions in Table 1 in terms of convenient nondimensional parameters. The parameter Q is the ratio of the anti-icing heating rate to the rate of heat loss by convection alone. The heat loss by convection alone is the heating rate required to maintain the surface at the same temperature in a dry environment. The parameter b is a non-dimensionalized liquid water impingement rate per unit area, hence, it is proportional to the freestream liquid water content, the flow rate of the freestream, and the capture efficiency of the surface upon which the subcooled droplets are impinging. Hence, b reflects the dependence of anti-icing heating rate on droplet-size distribution. In Figs. 3 and 4, the limiting value for b (0.0261) shown corresponds to the case

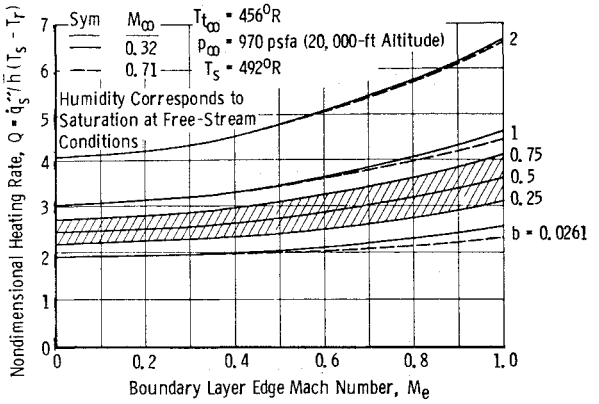

Fig. 3 Sensitivity of nondimensional heating rate Q to sensible heat parameter b.

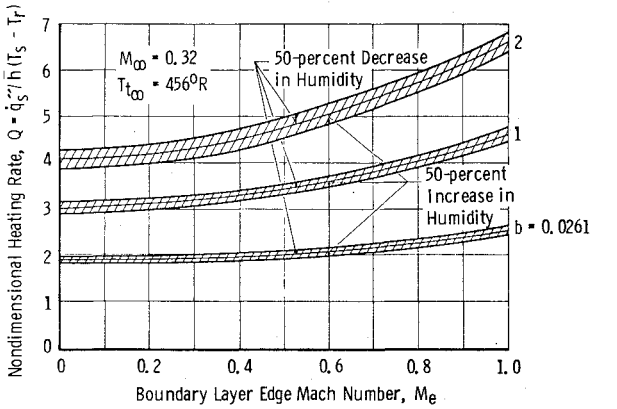

Fig 4 Sensitivity of nondimensional heating rate Q to humidity for different values of the sensible heat parameter b.

where the rate of liquid water impingement is equal to the rate of evaporation of water from the surface, assuming a continuous film of water over the surface.

Figure 3 shows the effects of boundary-layer edge Mach number M_e and the parameter b on the heating rate parameter Q for the high-altitude test conditions of the military specification given in Table 1. Calculations have shown that b for icing surfaces in a turbine engine generally will not exceed 2.0. If b is increased from 0.0261 to 2, Q only increases by a factor of 2 over the range of Mach numbers shown. This is an important result since b is directly proportional to the liquid water content and depends on the droplet-size distribution. For, if b is approximately 0.5, a 50% variation in b results in about a 10% variation in Q. It can be concluded that exact duplication of the liquid water content or capture efficiency is not too important in conducting tests on components with anti-icing heat. It has been pointed out[3] that this conclusion may not be valid when conducting tests on components without anti-icing heat or for testing de-icing equipment. The rate of ice accretion on an unheated surface is highly dependent on liquid water content and liquid capture rate; the frequency of operation, and therefore the heating load of a de-icing system, is a more sensitive function of the rate of ice accretion.

In Fig. 4, the effect of humidity on the heating rate parameter Q is shown. It can be noted that, for the flow conditions for which the calculations were made, the heating rate parameter is relatively insensitive to the freestream humidity. This effect is due to the low partial pressure of water vapor at the edge of the boundary layer under icing conditions compared with the partial pressure at the edge of the liquid film on the anti-icing surface. The partial pressure difference across the boundary layer, of course, determines the rate of mass evaporation from the film. Large variations in the relatively small partial pressure at the boundary-layer edge do not significantly affect the partial pressure difference. This result should not be interpreted to mean that control of humidity is unimportant when conducting any anti-icing test. There are two reasons for this remark. First, as will be shown later, the humidity of the airstream in the test facility has an important effect on the rate at which the icing spray cloud water droplets approach temperature equilibrium with the airstream because of evaporative cooling. Second, a wide range of humidity settings is usually possible in a test cell. At high subsonic flight Mach numbers, the specific humidity for saturation at the static conditions may be an order of magnitude lower than the specific humidity for saturation at the total conditions. A humidity difference of this magnitude may have a significant effect on the required anti-icing heating rate. It is for this reason that a humidity value for either specified total or specified static conditions should be included in engine icing qualification test specifications.

The effect of humidity on the heating rate parameter becomes more pronounced as the air temperature is increased, although the absolute heating load for the anti-icing system diminishes. This effect deserves detailed consideration if meaningful anti-icing tests are to be conducted at temperatures above −4°F.

Analysis of Flow in an Icing Test Cell

In this section, an analysis of the inlet flow conditions for a typical direct-connect type of turbine engine icing test cell is presented. Through a number of simplifying assumptions, the problem is reduced to an analysis of one-dimensional flow. The analysis provides a means for predicting the thermodynamic and kinetic state of the air-water mixture at the test section. It is used to determine the effect of thermodynamic state of the flow at the engine station for typical icing tests.

Development of the Flow Model

Figure 5 is a schematic of the icing test facility being considered. The duct has an arbitrary cross-sectional area, and water is injected parallel to and in the direction of the gas flow at some location along the duct. The analysis is based on the overall conservation of species, mass, momentum, and energy, both globally and in each phase.

The mathematical model for flow in the duct is based on the following assumptions and propositions: 1) All gases including water vapor are treated as ideal gases. 2) Flow is one dimensional. 3) The gas phase is homogeneous at any axial station except in the boundary layers of the droplets. 4) The droplet-size distribution of the spray can be characterized by discrete drop sizes. All droplets having diameter d_i form class i. 5) Droplets are injected parallel to and in the direction of the gas flow and remain entrained in the gas stream throughout the duct. That is, de-entrainment by gravity and turbulent diffusion is considered negligible. 6) Each droplet injected maintains its identity through the duct. Hence, collisions, agglomeration, and drop breakup are considered negligible. 7) Internal resistance to heat transfer within a droplet is much lower than external or film resistance to heat

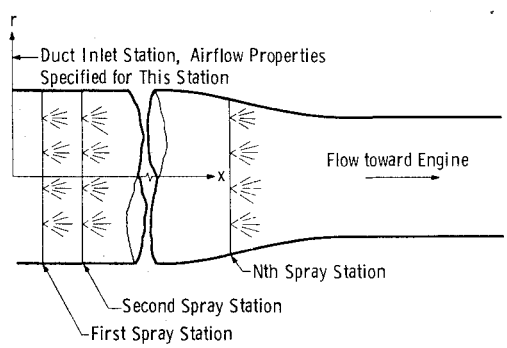

Fig. 5 Simplified schematic of duct geometry for analysis.

transfer. Thus, the internal temperature of a droplet is uniform at any instant of time. 8) Heat transfer and friction at the duct walls are negligible. 9) Cross-sectional area of the duct is a prescribed function of axial location. 10) The droplets are spherical in shape. 11) Droplets can be supercooled to a critical temperature which is a prescribed function of droplet diameter. 12) Upon reaching the critical temperature, the droplet suddenly becomes a mixture of ice and water at the normal bulk freezing temperature. The fraction of ice present is proportional to the degree of supercooling before the freezing process started. The droplet remains at the normal freezing temperature until enough heat has been removed to completely freeze the drop. After the drop freezes, it is treated as an ice particle. 13) Vaporization and condensation are occurring at any instant at equilibrium rates. That is, at any instant the drop surface vapor pressure is equal to the saturation pressure corresponding to droplet temperature. The droplets of interest in icing problems are large enough for the effect of surface tension on vapor pressure to be negligible. 14) The number of injection stations and their locations is arbitrary, but less than or equal to ten. The droplets injected at any station have uniform diameter, but the diameter can vary with injection station. By placing a number of injection stations close together, a distribution of discrete droplet sizes can be treated.

Based on these assumptions and propositions, the following global conservation equation can be written:

Conservation of mass

$$W_v + W_{nc} + \sum_i W_{c_i} = W = \text{constant} \tag{3}$$

Conservation of water (condensed phase plus vapor)

$$W_v + \sum_i W_{c_i} = W_{w_t} = \text{constant} \tag{4}$$

Conservation of noncondensable gas

$$W_{nc} = V_g \rho_g (1 - C_v) A = \text{constant} \tag{5}$$

Conservation of momentum

$$V_g^2 \frac{dC_v}{dx} + (1 - C_v) V_g \frac{dV_g}{dx} + V_g (1 - C_v)^2 \times \sum_i \left[V_{c_i} \frac{df_{c_i}}{dx} + f_{c_i} \frac{dV_{c_i}}{dx} \right] + \frac{(1 - C_v)}{\rho_g} \frac{dP}{dx} = 0 \tag{6}$$

Conservation of energy

$$\frac{dh_{nc}}{dx} + V_g \frac{dV_g}{dx} + \frac{(h_v + V_{g/2}^2)}{(1 - C_v)^2} \frac{dC_v}{dx} + \frac{C_v}{(1 - C_v)} \left[\frac{dh_v}{dx} + V_g \frac{dV_g}{dx} \right] + \sum_i (h_{c_i} + V_{c_i/2}^2) \frac{df_{c_i}}{dx} + \sum_i f_{c_i} \left[\frac{dh_{c_i}}{dx} + V_{c_i} \frac{dV_{c_i}}{dx} \right] = 0 \tag{7}$$

Mass, momentum and energy transfer between phases can be treated by first considering these processes for a single droplet. For a droplet of class i, the following conservation equations apply:

Conservation of mass

$$V_{c_i} \frac{dM_{d_i}}{dx} = k_{x_i} \pi d_i^2 \bar{M}_v \frac{x_v - (x_{v_s})_i}{1 - (x_{v_s})_i} \tag{8}$$

Conservation of momentum

$$M_{d_i} V_{c_i} \frac{dV_{c_i}}{dx} + (V_{c_i} - V_g) V_{c_i} \frac{dM_{d_i}}{dx} = \rho_g \frac{\pi d_i^2}{4} C_{D_i} |V_g - V_{c_i}| (V_g - V_{c_i})/2 \tag{9}$$

Conservation of energy

$$V_{c_i} \frac{dE_{c_i}}{dx} = \bar{h}_i \pi d_i^2 [T_\infty - (T_s)_i] + h_{v_{s_i}} V_{c_i} \frac{dM_{d_i}}{dx} \tag{10}$$

By considering all droplets of class i

$$\frac{df_{c_i}}{dx} = \frac{f_{c_i}}{M_{d_i}} \frac{dM_{d_i}}{dx} \tag{11}$$

and

$$\frac{d(h_{c_i} W_{c_i})}{dx} = \frac{W_{c_i}}{M_{d_i}} \frac{dE_{c_i}}{dx} \tag{12}$$

For low rates of mass transfer, the heat and mass transfer coefficients for spherical droplets can be obtained from the semi-empirical equations of Ranz and Marshall.[9] Thus

$$k_{x_i} = \frac{\mu}{d_i S_c \bar{M}_v} (2.0 + 0.6 Re_i^{1/2} S_c^{1/3}) \tag{13}$$

and

$$\bar{h}_i = \frac{\mu C_p}{d_i Pr} (2.0 + 0.6 Re_i^{1/2} Pr^{1/3}) \tag{14}$$

where the Reynolds number is given by

$$R_{e_i} = |V_g - V_{c_i}| \rho_g d_i / \mu \tag{15}$$

Carlson and Hoglund[10] determined the following semi-empirical equation for the drag coefficient of a solid sphere in low-speed flow in the absence of mass transfer

$$C_{D_i} = (24/Re_i)(1.0 + 0.15\, Re_i^{0.687}) \tag{16}$$

This relation is assumed to be valid for low rates of surface mass transfer as well. The previous transport equations are used in the present study although the rates of mass transfer immediately following droplet injection may be high.

Also required in the solution processes are the thermodynamic property data for air, water vapor, liquid water, and ice. Empirical correlation functions were obtained from pertinent literature.[3]

Property data for air

$$C_{p_{nc}} = 0.2318 + 0.1040 \times 10^{-4} T + 0.7166 \times 10^{-8} T^2 \tag{17}$$

$$h_{nc} = 0.2318T + 0.520 \times 10^{-5} T + 0.2389 \times 10^{-8} T^3 - 127.064 \tag{18}$$

Valid for $400 \leq T \leq 1700$

Property data for water vapor

$$C_{pv} = 0.4451 + 0.9071 \times 10^{-4} T - 0.211097 \times 10^{-7} T^2 \quad (19)$$

$$h_v = 848.3 + 0.4451T + 0.45355 \times 10^{-4} T^2 - 0.70366 \times 10^{-8} T^3 \quad (20)$$

Valid in the range $400 \leq T \leq 1700$

Specific heat data of the liquid water and ice

$$C_c = 1.0 \quad (21a)$$

$$C_{cs} = 0.485 \quad (21b)$$

Vapor pressure of the condensed phases

The vapor pressure of liquid water in the range $492 \leq T \leq 672$ was given by

$$P_v = 2117.0 \left\{ \frac{672}{T} \right\}^{4.901} \exp\left\{ -9.06 \left[\frac{h_{fg}}{T} - 1.45257 \right] \right\} \quad (22)$$

where $h_{fg} = 1352.3 - 0.5696T + 0.839 \times 10^{-5} T^2 + 0.927 \times 10^{-8} T^3$ The vapor pressure for supercooled liquid water, $T \leq 492$, was given by

$$P_v = 2117.0 \exp\left[2.3 \left\{ A_1 + \frac{B_1}{t} + \frac{C_1 (t^2 - K_1)}{t} \times [10^{(D_1(t2-k_1)^2)} - 1.0] + E_1 [10^{(F_1(374.11-t)^{5/4})}] \right\} \right] \quad (23)$$

where $A_1 = 5.4266514$; $B_1 = -2.0051 \times 10^3$; $C_1 = 1.3869 \times 10^{-4}$; $D_1 = 1.1965 \times 10^{-11}$; $E_1 = -4.4 \times 10^{-3}$; $F_1 = -5.7148 \times 10^{-3}$; $K_1 = 2.937 \times 10^5$. The vapor pressure for ice was given by

$$P_v = 2.7845 \exp[2.3\{ (A_2/t) + 0.4343 B_2 \log_e t + C_2 t + D_2 t^2 + E_2 \}] \quad (24)$$

where $A_2 = -2.4455646 \times 10^3$; $B_2 = 8.2312$; $C_2 = -1.677006 \times 10^{-2}$; $D_2 = 1.20514 \times 10^{-5}$; $E_2 = -6.757169$.

It should be remarked that the thermodynamic property data, such as the water vapor enthalpy, as expressed by quadratic or cubic polynomials will differ from exact property data[11] slightly over certain portions of their applicable range. But since energy balances or heat transfer or mass transfer are based on differences or the ratio of differences of properties, these slight curve fit errors or the usage of different base reference states cause no substantial computational errors. Note that the units of p_v are psfa, those of C and c_p are Btu/lbm-°R, and h_{nc}, h_{fg}, and h_v are Btu/lbm. The temperatures used are either T°R or t°K. The gas viscosity μ is defined as a mole average viscosity. The functions giving the air and water vapor viscosity are, respectively

$$\mu_{nc} = (7.5 \times 10^{-7} T^{1/2}) / (1 + \frac{216.0}{T}) \quad (25)$$

and

$$\mu_v = (10.6 \times 10^{-7} T^{1/2}) / (1 + \frac{1538.0}{T}) \quad (26)$$

Their units are lbm/(ft-sec)

Finally, the critical droplet freezing temperatures are assumed to be only functions of the droplet diameter. For the study[3] reported herein, the relationship assumed was

$$T_f = 463.2°\text{R} \text{ for } 300 \leq d \leq 1000 \quad (27)$$

and

$$T_f = [463.2 + 16.32 \log_e (0.003333\, d)]°\text{R} \quad d \leq 300 \quad (28)$$

where d is the droplet diameter in microns.

These governing differential equations were programed in FORTRAN IV language for numerical solution on a digital computer. The modified Euler method of integration was used in the solution. To obtain a solution, the duct shape and inlet flow conditions must be known. The inlet flow variables which must be specified are gas temperatures and velocity, static pressure, vapor mass fraction, liquid temperature and velocity, droplet diameter, and liquid mass fraction.

Application of the Flow Model

To determine the influence of the test cell inlet conditions on the thermal and kinetic state at the engine test section, a parametric study was performed using the test cell flow model. The particular duct (test cell) geometry chosen for the study is shown in Fig. 6. The bell-mouth entrance approximates the inlet section of the AEDC Propulsion Engine Test Cell (J-1) and typifies many other installations.

Calculations were made for several sets of typical icing test conditions, and some results worthy of note were observed. These results are believed to be applicable to most practical icing test conditions for turbine engines. Figure 7 illustrates temperature, liquid water content, and humidity distributions in the duct for one set of inlet conditions. These conditions correspond to a high engine power setting and high subsonic flight Mach number at 20,000-ft alt with a total temperature of −4°F relative to the aircraft. The initially rapid approach to equilibrium is especially evident. Almost all of the droplet temperature change occurs within 1 ft of the water injection station. As a general rule, it has been found that the flow properties become essentially constant within 20 ft for droplet diameters less than 40μ. Droplets rapidly approach the wet-bulb temperature corresponding to the local humidity. Of course, if the duct is sufficiently long, the air will become saturated, and thermodynamic equilibrium will be obtained. The approach to equilibrium beyond about 1 ft is extermely slow because of the low droplet heat and mass transfer coefficients. In general, the evaporation rate is limited by the rate of heat transfer to the droplets since the latent heat of vaporization is so large. The initially high vaporization rate is associated with the sensible energy possessed by the droplets at injection and readily available to supply the latent heat necessary for evaporation.

For a flight Mach number of 0.32, the corresponding atmospheric temperature is 447°R, and the vapor mass fraction

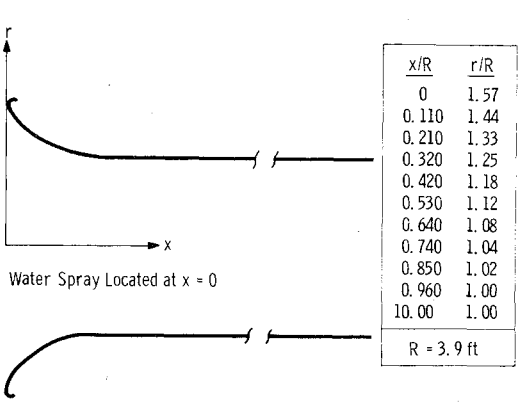

Fig. 6 Duct geometry used in the parametric study of this report.

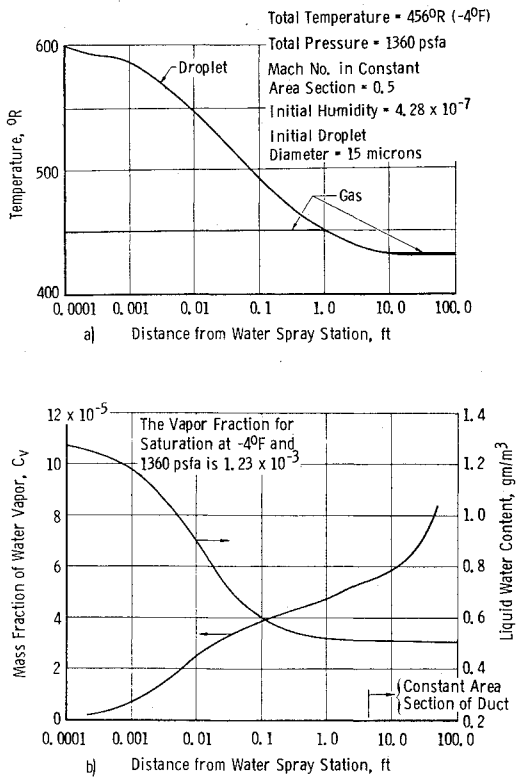

Fig. 7 Variations in flow properties vs axial position; a) temperatures; b) vapor mass fraction and liquid water content.

for saturation is about 110×10^{-5}. In order to illustrate the humidification of the gas stream by the spray system, Fig. 7 was prepared. The inlet air water vapor fraction was selected to be approximately zero (4.28×10^{-7}). From Fig. 7b, it can be noted that downstream at about 15 ft from the injector the total change in humidity is only about 10% of the humidity necessary for saturation at the static conditions corresponding to the duct Mach number, 0.5. This points out the danger of attempting to establish the humidity of the flow at the engine station by vaporization of the liquid water sprayed into the duct.

The parametric study revealed that the thermodynamic state 20 ft beyond the inlet is relatively insensitive to the inlet water temperature, velocity and the liquid water content. As one could expect, the thermodynamic state was found to be sensitive to inlet air temperature and pressure and to a lesser degree sensitive to the inlet humidity. Some dependence of the thermodynamic state on the relative velocity between the air and water droplets at the injection station was observed at low relative velocities. Beyond 20 ft, droplet-size distribution was observed to have small effect on the fluid state, and either the mass mean or mass median diameter can be used to characterize the distribution for a calculation of the state. This result applies to drop size distributions that characterize icing environments, that is, like those of Fig. 2.

Conclusions

A study of icing simulation for turbine engines in altitude test cells was made. Several aspects of the icing problem were analyzed and discussed.

An analysis of the heating rate required to maintain an anti-icing condition on a surface was made. From the analysis, it was determined that the heating rate is relatively insensitive to droplet-size distribution and liquid water content and only moderately sensitive to humidity. It can be concluded that exact duplication of these variables is not required for adequate testing of an anti-icing system. Icing tests in the absence of anti-icing heat and the testing of de-icing systems will generally require better simulation of the environment than testing under anti-icing conditions.

From a simplified analysis of droplet capture efficiency on bodies representing various turbine engine components, it was found that the overall capture efficiencies are relatively insensitive to droplet-size distributions shown in Fig. 2. The mass median diameter was sufficient to characterize the droplet-size distribution for capture efficiency.

A mathematical model for the flow in a typical direct-connect type of turbine engine test cell was developed and the governing equations were programed for computer solution. The results of the calculations indicate that simulation of icing conditions at the face of an engine compressor can be obtained through proper selection of the test cell inlet conditions and water spray settings. The model can be used to evaluate test cell inlet conditions for proper simulation. The thermodynamic state at the engine was found to be sensitive to inlet air temperature, pressure, and humidity and insensitive to the inlet water temperatures, droplet-size distribution and velocity, and liquid water content. The velocity difference between the inlet airflow and the water from the spray system was relatively important, however, in its effect on droplet heat and mass transfer.

In general, the total pressure and temperature at the test cell inlet should be set equal to the total pressure and temperature of the free flight condition being simulated. There is some humidification from the water spray system but in most cases this influence can be ignored. Hence, in usual practice for anti-icing tests, test cell inlet specific humidity should be set equal to the specific humidity corresponding to saturation at the static pressure (altitude) and static temperature being simulated. However, the humidity setting may be much more important in de-icing studies and power-off icing tests requiring more precise establishment. This aspect requires further study. The test article should be located sufficiently far downstream of the spray section to ensure that the required near-equilibrium thermal state is obtained in the test section. The required minimum distance can be calculated using a mathematical model and computer program like that developed in this study. For the system considered in this study, the distance was approximately 20 ft. The results show that current capability to provide icing environments for turbine engine testing in altitude test cells is quite adequate.

References

[1] Kissling, H.H., "Aircraft Engine Anti-Icing Test and Evaluation Technology," presented at AIAA 10th Aerospace Science Meeting, San Diego, Calif.

[2] Striebel, E.E., "Ice Protection for Turbine Engines," Rept. AD690469, Federal Aviation Agency, Washington, D.C., 1969.

[3] Willbanks, C.E. and Schulz, R.J., "Analytical Study of Icing Simulation for Turbine Engines in Altitude Test Cells," AEDC-TR-73-144, Nov., 1973, Arnold Engineering Development Center, Tullahoma, Tenn.

[4] Battan, L.J. and Reitan, C.H., "Droplet Size Measurements in Convective Clouds," *Proceedings of the First Conference on the Physics of Clouds – Artificial Stimulation of Rain,* 1958.

[5] Gall, E.S. and Floyd, F.X., "Icing Test Capability of the Engine Test Facility Propulsion Development Test Cell (J-1)," AEDC-TR-71-94 (AD729205), Aug. 1971, Arnold Engineering Development Center, Tullahoma, Tenn.

[6] Langmuir, I. and Blodgett, K., "A Mathematical Investigation of Water Droplet Trajectories," Air Material Command Tech. Rept. 5418, Feb. 1946, Army Air Force.

[7] Dorsch, R.G., Brun, R.J., and Gregg, J.L., "Impingement of Water Droplets on an Ellipsoid with Fineness Ratio 5 in Axisymmetric Flow," NACA TN 3099, March 1954.

[8] Neel, C.B., Jr., Bergum, N.R., Jukoff, D., and Schlaff, B.A., "The Calculation of the Heat Required for Wing Thermal Ice Prevention in Specified Icing Conditions," NACA TN 1472, Dec. 1947.

[9] Ranz, W.E. and Marshall, W.R., "Evaporation from Drops—Part II," *Chemical Engineering Progress,* Vol. 48, No. 4, April 1952, pp. 173-180.

[10] Carlson, D.J. and Hoglund, R.F., "Particle Drag and Heat Transfer in Rocket Nozzles," *AIAA Journal,* Vol. 2, Nov. 1964, pp. 1980-1984.

[11] Keenan, J.H., Keyes, F.G., Hill, P.G., and Moore, J.G., *Steam Tables,* (English Units), Wiley, New York, 1969.